INVESTIGATION OF THE EFFECT OF THE WAKE GENERATED BY ROTOR BLADES ON THE FLOW THROUGH STATOR PASSAGE FOR LOW PRESSURE TURBINE

Prof. Dr. Ihsan Y. Hussain
Mech.Engr.Dept.
College of Engineering
University of Baghdad
Baghdad-Iraq

Dr.Ahmed W. Mustafa
Mec.Eng.Dept.
College of Engineering
University of Tikrit

ABSTRACT

The effects of incoming wakes of upstream rotor on the flow field in a low pressure turbine cascade are investigated. The flow field is studied numerically with and without inlet wake. The rotor effect is represented by moving bars that produce passing wakes at the entrance of the stator. The flow field is analyzed numerically by solving the steady and unsteady forms of the two-dimensional compressible Reynolds-averaged Navier-Stokes equations. Steady flow is performed without wake while the unsteady flow is performed with periodic inlet wake for Reynolds number of order 10^5. A k-ε turbulence model is used to obtain the eddy viscosity. The Cartesian velocity components and pressure on a collocated (non-staggered) grid are used as dependent variables in the momentum equations, which discretized by finite volume method, body fitted coordinates are used to represent the complex blade geometry accurately, and grid generation technique based on elliptic partial differential equations is employed. **SIMPLE** algorithm is used to adjust the velocity field to satisfy the conservation of mass. The results show that the wake passing produces unsteady pressure field in the direction of the rotor traverse. The comparison with the experimental data is acceptable and there is similar trend between the prediction and experimental data, except at the separation flow region due to the limitation of the turbulence model.

الخلاصة

تاثيرات الاعقاب (wakes) القادمة من الدوار على حقل الجريان في سلسلة ريشات (cascade) توربين منخفض الضغط تم تحريها. حقل الجريان تم دراستة عدديا بوجود وبعدم وجود اعقاب عند المدخل. تاثير الدوار تم تمثيله بواسطة اعمدة متحركة تنتج اعقاب عند مدخل الثابت. تم تحليل حقل الجريان عدديا بحل معادلات (Reynolds-averaged Navier Stokes) الثنائية الابعاد والانضغاطية للحالة المستقرة وغير المستقرة. الحالة المستقرة انجزت بعدم وجود اعقاب بينما الحالة الغير مستقرة انجزت بوجود اعقاب دورية عند المدخل لرقم رينولد من رتبة 10^5 . نموذج اضطراب (k-ε) تم استخدامه للحصول على اللزوجة الدوامية. مركبات السرع الديكارتية والضغط على شبكة متحدة الموقع تم استخدامها كمتغيرات معتمدة في معدلات الزخم التي تم تقطيعها بطريقة الحجم المحدد, احداثيات مطابقة الجسم تم استخدامها لتمثيل شكل الريشة المعقد بشكل دقيق, وتم استخدام طريقة توليد الشبكة على اساس معادلات تفاضلية جزئية بيضوية. خوارزمية SIMPLE

استخدمت لتعديل حقل السرعة لكي تحقق حفظ الكتلة. بينت النتائج ان الاعقاب المارة تنتج حقل ضغط غير مستقر باتجاة حركة الدوار. المقارنة مع البيانات العملية مقبولة وهناك تشابة في ميل او اتجاة البيانات العملية مع النتائج المحسوبة , ما عدا منطقة الانفصال بسبب تحديد نموذج الاضطراب.

KEYWORDS: Wake, Low Pressure Turbine, Collocated Grid, Unsteady Flow

INTRODUCTION

Flow in an axial turbine blade rows is highly unsteady (with the exception of the first stator blade), because they periodically encounter flow distortions generated by upstream blade rows and combustors. This unsteadiness has important consequences for the turbine stage efficiency, blade loading, mechanical fatigue, heat transfer, thermal fatigue and noise generation. The induced unsteady flow depends upon the scale of the upstream disturbance like wakes. These unsteady flow-generating factors can be classified based on the physical mechanisms involved as: -

- Potential Interaction of Upstream and Downstream Rows.

Potential interactions arise because the entire blades have circulation and therefore a potential field propagates throughout the space. The magnitude of this effect depends on a number of factors. (**Parker and Watson, 1972),** gave series of relationships for unsteady pressure and velocity for two-dimensional cascade; the potential field associated with blade row propagates both upstream and downstream pressure and it varies approximately in proportion to the quantity ($\exp(-2\pi\sqrt{1-M^2}\,\frac{x}{s})$), where "*x*" is the axial distance from the blade row, "*s*" is the pitch of the blade row and "*M*" is the local Mach number. This equation means that in high Mach number flows, potential interactions will tend to be stronger than lower speed. If the Mach is high enough, then the potential field will propagate without decay. (**Parker and Watson, 1972)** confirmed that the effects of potential interactions would be insignificant for axial spacing greater than about 30% of the blade pitch. As the flow in the current study is subsonic with minimum blade row axial gap of about 25% in the present study, this potential interaction will be neglected.

- Wake-Blade Interaction.

One of the first studies of the interaction of wake with blade was conducted by **(Meyer, 1958),** who used thin airfoil theory and he presented a solution for the interaction of the upstream blade wake with moving downstream blade row. Each wake is initially represented as a perturbation of the uniform flow. The wakes are transported with the main flow and chopped into segments by the downstream blade row. Inside the blade passage, the wake continues to behave as a negative jet. The velocity induced by the negative jet causes a build up of the wake fluid on the suction surface and removal of the wake fluid from the pressure surface. **(Hodson, 1985)** developed a numerical solution to predict the unsteady wake-blade interaction phenomena observed in his experimental investigation. He used a two-dimensional inviscid formulation based on that of (**Denton, 1983),** who used time marching calculation. In the absence of any real viscous forces, artificial viscosity was used to model the viscous decay of the wake. He showed that the unsteadiness in the turbine passage determined by the convection phenomena associated with passing wakes through the passage. **(Giles, 1987)** also developed a numerical solution for calculating the two-dimensional inviscid flow of the wake-blade interaction. He solved the two-dimensional Euler equations using Lax-Wendroff method. His results were similar to those of (**Hodson, 1985)**. **(Reda, 1989)** performed a numerical solution for predicting the flow between parallel plates subject to moving wake generated by moving

cylinders at the entrance of the channel. He solved the two-dimensional unsteady incompressible Navier Stokes Equations on a staggered grid and the eddy viscosity was obtained by using a k-ε model. The results showed that the upstream wakes produces a pressure field at the stator entrance that increases in the direction of the wake traverse and large oscillations in the mean velocities were introduced due to wake passing. **(Hodson and Dawes, 1998)** developed a numerical solution to predict the flow in turbine passage subject to passing wake at the inlet of the cascade. They solved the two-dimensional unsteady Reynolds Averaged Navier Stokes equations on unstructured mesh. They used low Reynolds number k-ε model to calculate the eddy viscosity. The results showed that the fluctuations in stagnation pressure and stagnation temperature downstream are greater than the defects that occur in the wake at the inlet of the blade row. **(Stieger, 2002)** has made measurements of the convection of turbulent wakes at the mid-span of a low-pressure linear cascade using 2D (Laser Doppler Anemometry LDA). The turbine blade in the cascade subject to incoming turbulent wakes; moving bars fitted between two belts generated these wakes. The wake generator is driven by a motor by means of mechanism of belts and pulleys and provides linear motion of the bars as shown in **Fig. (1)**. He used high response pressure transducers (Kulite) for pressure surface measurements. The measurements confirmed that the wake fluid convected through the blade passage.

GOVERNING EQUATIONS

The present work considers the unsteady turbulent flow between stator turbine blade, the mass conservation and the Reynolds-averaged momentum equations are written in Cartesian tensor form as :-

$$\frac{\partial \overline{\rho}}{\partial t}+\frac{\partial}{\partial x_j}\left(\overline{\rho u_j}\right)=0 \tag{1}$$

$$\frac{\partial}{\partial t}\left(\overline{\rho u_i}\right)+\frac{\partial}{\partial x_j}\left(\overline{\rho u_i u_j}\right)=-\frac{\partial \overline{p}}{\partial x_i}+\frac{\partial}{\partial x_j}\left[\left(\mu+\mu_t\right)\left(\left(\frac{\partial u_i}{\partial x_j}+\frac{\partial u_j}{\partial x_i}\right)-\frac{2}{3}\frac{\partial u_k}{\partial x_k}\delta_{ij}\right)\right]-\frac{2}{3}\rho k\delta_{ij} \tag{2}$$

Where ρ is the mean density, u_j the mean velocity, and p the mean pressure. From the k-ε turbulence model, **(Launder and Spalding, 1974)**, the turbulence viscosity μ_t is given by:-

$$\mu_t = C_\mu \frac{\rho k^2}{\varepsilon} \tag{3}$$

Where k is the turbulence kinetic energy and ε is the turbulence energy dissipation. The model is then composed of two equations; one for k and another for ε presented as follows: -

$$\frac{\partial}{\partial t}\left(\overline{\rho k}\right)+\frac{\partial}{\partial x_j}\left(\overline{\rho k u_j}\right)=\frac{\partial}{\partial x_j}\left[\left(\mu+\frac{\mu_t}{\sigma_k}\right)\frac{\partial \overline{k}}{\partial x_j}\right]+P_k-\overline{\rho\varepsilon} \tag{4}$$

$$\frac{\partial}{\partial t}\left(\overline{\rho\varepsilon}\right)+\frac{\partial}{\partial x_j}\overline{\rho\varepsilon u_j}=C_{\varepsilon 1}\frac{\overline{\varepsilon}}{k}P_k+\frac{\partial}{\partial x_j}\left[\left(\mu+\frac{\mu_t}{\sigma_\varepsilon}\right)\frac{\partial\overline{\varepsilon}}{\partial x_j}\right]-C_{\varepsilon 2}\overline{\rho}\frac{\overline{\varepsilon^2}}{k} \quad (5)$$

Where P_k is the rate of production of turbulence kinetic energy, given by:-

$$P_k=\mu_t\left[\left(\frac{\partial\overline{u_i}}{\partial x_j}+\frac{\partial\overline{u_j}}{\partial x_i}\right)\right]\frac{\partial\overline{u_i}}{\partial x_j}-\frac{2}{3}\frac{\partial\overline{u_i}}{\partial x_j}\delta_{ij}\left[\mu_t\frac{\partial\overline{u_k}}{\partial x_k}+\overline{\rho k}\right] \quad (6)$$

This model contains five empirical constants which assume the following values:-

$$C_\mu=0.09, C_{\varepsilon 1}=1.45, C_{\varepsilon 2}=1.9, \sigma_k=1.0, \sigma_\varepsilon=1.3$$

BOUNDARY CONDITIONS

For the steady state there are four types of boundaries in the physical flow domain, inlet, outlet, solid surfaces and periodic boundary as shown in **Fig.(2)**. At the inlet of the cascade the velocity components and turbulent kinetic energy are specified, Pressure is assumed to be unchanging in the flow direction at the inlet, therefore the inlet should be located far enough upstream of the blade row to ensure that this assumption is valid. At the exit plane the values of the dependent variables are unknown. Therefore the outlet boundary should be placed far down from the region of interest, at a location where the flow properties are not varied. The outlet properties can be found by set the streamwise derivatives (gradients) of all unknown variables to zero. All the velocity components are set to zero on all solid boundaries (blade surfaces and end walls). Wall pressure is determined by setting the pressure gradient normal to the surface equal to zero. The turbulence scalar transport equations (4 and 5) are only valid for fully turbulent regions. An additional model must be introduced to treat the laminar sublayer region. The wall function method is used in the present study to eliminate the large number of grid points needed to resolve the laminar sublayer more detail about the wall function are available in **(Ahmed, 2005)**. The cyclic or periodic boundary condition is a type of symmetry boundary condition. When applying this boundary condition, it is required to set the flux of all variables leaving the outlet cyclic boundary equal to the flux entering the inlet cyclic boundary on the opposite side.

SIMULATION OF THE UNSTEADY FLOW

In an effort to remove some of geometrical and physical complexity associated with the unsteady flow in the turbine cascade **(Fig.3a)**, **(Stieger, 2002),** investigated experimentally the wake blade interaction such that the wakes shed from the upstream rotor in a real machine are simulated by an array of cylindrical bars moving in the traverse direction in the stator inlet plane as shown in **(Fig.3b)**, these wakes causes unsteadiness in the stator passage. **Schlichting (1968)** proposed a solution of turbulent wake behind a stationary bar, gave the solution of wake behind cylinder as: -

$$\frac{U(x,y)}{U_\infty} = 1 - \left[\frac{\Delta U_{\max}}{U_\infty} \left(1 - \left(\frac{y}{b} \right)^{\frac{3}{2}} \right)^2 \right] \tag{7}$$

Where

$$\left. \begin{aligned} \frac{\Delta U_{\max}}{U_\infty} &= 0.98 \sqrt{\frac{C_d d}{x}} \\ b &= 0.576 \sqrt{C_d x d} \end{aligned} \right\} \tag{8}$$

Where d is the diameter of the cylinder, C_d is the drag coefficient of the cylinder, and b is half-wake width.

In the present study, as the cylinders are moving at the inlet plane the decay laws are transformed to the coordinates of wake frame of reference, therefore equation (7) and (8) can be written as: -

$$\frac{U_r(x_r, y_r)}{U_\infty} = 1 - \left[\frac{\Delta U_{\max}}{U_\infty} \left(1 - \left(\frac{y_r}{b} \right)^{\frac{3}{2}} \right)^2 \right] \tag{9}$$

$$\left. \begin{aligned} \frac{\Delta U_{\max}}{U_\infty} &= 0.98 \sqrt{\frac{C_d d}{x_r}} \\ b &= 0.576 \sqrt{C_d x_r d} \end{aligned} \right\} \tag{10}$$

Where

$$\left. \begin{aligned} x_r &= x \cos\alpha_r + y \sin\alpha_r \\ y_r &= y \cos\alpha_r - x \sin\alpha_r \end{aligned} \right\} \tag{11}$$

And the velocity components in the wake are obtained as: -

$$\left. \begin{aligned} U_x(wake) &= U_r(x_r, y_r) \cos\alpha_r \\ U_y(wake) &= U_r(x_r, y_r) \sin\alpha_r - U_{bar} \end{aligned} \right\} \tag{12}$$

TRANSFORMATION OF THE GOVERNING EQUATIONS

The set of conservation equation typically can be written in the Cartesian system of coordinates for a scalar transport as: -

$$\frac{\partial(\rho\phi)}{\partial t}+\frac{\partial(\rho u\phi)}{\partial x}+\frac{\partial(\rho v\phi)}{\partial y}=\frac{\partial}{\partial x}\left(\Gamma^{\phi}\frac{\partial\phi}{\partial x}\right)+\frac{\partial}{\partial y}\left(\Gamma^{\phi}\frac{\partial\phi}{\partial y}\right)+S_{\phi} \quad (13)$$

Where

(ϕ) is any dependent variable.

(Γ^{ϕ}) is the exchange coefficient of ϕ.

(S_{ϕ}) is the source term of ϕ.

Equation (14) can be transformed from physical domain to computational domain according to the following transformation:-

$$\left.\begin{aligned}\varsigma&=\varsigma(x,y)\\ \eta&=\eta(x,y)\\ \tau&=t\end{aligned}\right\} \quad (14)$$

The final form of the transformed equation can be written as, **(Ahmed, 2005)**:-

$$\frac{\partial}{\partial\tau}\left(\frac{\rho\phi}{J}\right)+\frac{\partial}{\partial\varsigma}(\rho\phi G_1)+\frac{\partial}{\partial\eta}(\rho\phi G_2)=\frac{\partial}{\partial\varsigma}\left(\Gamma^{\phi}J\alpha\frac{\partial\phi}{\partial\varsigma}\right)+\frac{\partial}{\partial\eta}\left(\Gamma^{\phi}J\gamma\frac{\partial\phi}{\partial\eta}\right)+S_{\varsigma,\eta} \quad (15)$$

$$+\frac{S_{\phi}}{J}$$

Where

$$\left.\begin{aligned}&\alpha=\left(\frac{\partial x}{\partial\eta}\right)^2+\left(\frac{\partial y}{\partial\eta}\right)^2,\ \beta=\left(\frac{\partial x}{\partial\varsigma}\frac{\partial x}{\partial\eta}\right)+\left(\frac{\partial y}{\partial\varsigma}\frac{\partial y}{\partial\eta}\right)\\ &\gamma=\left(\frac{\partial x}{\partial\varsigma}\right)^2+\left(\frac{\partial y}{\partial\varsigma}\right)^2,\ G_1=u\frac{\partial y}{\partial\eta}-v\frac{\partial x}{\partial\eta}\\ &G_2=v\frac{\partial x}{\partial\varsigma}-u\frac{\partial y}{\partial\varsigma},\ J=1/(\frac{\partial x}{\partial\varsigma}\frac{\partial y}{\partial\eta}-\frac{\partial y}{\partial\varsigma}\frac{\partial x}{\partial\eta})\end{aligned}\right\} \quad (16)$$

And $S_{\zeta,\eta}$ is the source term due to the non-orthogonal and defined as: -

$$S_{\varsigma,\eta}=-\left(\frac{\partial}{\partial\eta}\left(\Gamma^{\phi}J\beta\frac{\partial\phi}{\partial\varsigma}\right)+\frac{\partial}{\partial\varsigma}\left(\Gamma^{\phi}J\beta\frac{\partial\phi}{\partial\eta}\right)\right) \quad (17)$$

NONDIMENSIONALIZATION OF THE GENERAL EQUATION

To obtain the flow behavior around bodies of similar shape with minimum computational effort it is desirable to group all the parameters, such as the body length and freestream velocity, into nondimenional numbers. Two flows are dynamically similar if the nondimensional numbers that govern the flows have the same value,

even though the parameters contained in the nondimensional numbers have different values. The best way to identify the appropriate nondimensional groups is to nondimensionalize the governing equations. So that in the present study the general transformed equation (4.24) is nondimensionalized by using the following scales: -

Length scale	axial chord length (C_x)
Time scale	Wake passing time (t_w)
Velocity scale	freestream velocity (U_∞)
Density scale	freestream density (ρ_∞)
Pressure scale	($\rho_\infty U^2_\infty$)
K.E. of turbulence	(U^2_∞)
Dissipation of K.E.	(U^3_∞ / C_x)

By using the above scales the nondimensional transport equation can be written as: -

$$\Omega \frac{\partial}{\partial \tau^*}\left(\frac{\rho^*\phi^*}{J^*}\right)+\frac{\partial}{\partial \varsigma^*}\left(\rho^*\phi^* G_1^*\right)+\frac{\partial}{\partial \eta^*}\left(\rho^*\phi^* G_2^*\right)=\frac{\partial}{\partial \varsigma *}\left(\Gamma^{\phi^*} J^* \alpha^* \frac{\partial \phi^*}{\partial \varsigma^*}\right)$$
$$+\frac{\partial}{\partial \eta^*}\left(\Gamma^{\phi *} J^* \gamma^* \frac{\partial \phi^*}{\partial \eta^*}\right)+S^*_{\varsigma,\eta}+\frac{S^*_{\phi^*}}{J^*} \qquad (18)$$

Where (Ω) is the reduced frequency and defined as ($\Omega = C_x / U_\infty t_w$). **Table (1)** summarizes ϕ^*, Γ^{ϕ^*} and $S^*_{\phi^*}$ for each transport equation used in the present work.

DISCRETIZATION OF THE GOVERNING EQUATIONS

The discretized governing equations are obtained by using a finite volume method on o non-staggered grid as discussed in the previous section. By integrating the general governing equation (19) over the control volume, we get: -

$$\int_{\tau^*}\int_{V^*}\Omega\frac{\partial}{\partial\tau^*}\left(\frac{\rho^*\phi^*}{J^*}\right)dV^*d\tau^*+\int_{\tau^*}\int_{V^*}\left[\frac{\partial}{\partial\varsigma^*}\left(\rho^*\phi^*G_1{}^*\right)+\frac{\partial}{\partial\eta^*}\left(\rho^*\phi^*G_2{}^*\right)\right]dV^*d\tau^*$$
$$=\int_{\tau^*}\int_{V^*}\left[\frac{\partial}{\partial\varsigma*}\left(\Gamma^{\phi^*}J^*\alpha^*\frac{\partial\phi^*}{\partial\varsigma^*}\right)+\frac{\partial}{\partial\eta^*}\left(\Gamma^{\phi*}J^*\gamma^*\frac{\partial\phi^*}{\partial\eta^*}\right)\right]dV^*d\tau^*$$
$$+\int_{\tau^*}\int_{V^*}\left[S^*_{\varsigma,\eta}+\frac{S^*_{\phi^*}}{J^*}\right]dV^*d\tau^* \qquad (19)$$

Using the upwind scheme to interpolate the convection terms and Euler implicit for time term and central scheme for diffusion and source terms, (the details of discretization of equation (19) are found in **(Ahmed, 2005)**, the final discretized equation can be written as: -

$$\phi_P^*A_P=\phi_E^*A_E+\phi_W^*A_W+\phi_N^*A_N+\phi_S^*A_S+\Omega\frac{\left(\frac{\rho_P^*\phi_P^*}{J_P^*}\right)^{\tau^*}}{\Delta\tau^*}+S_{total} \qquad (20)$$

Where

$$\left.\begin{aligned}
&A_E=\max\left(-F_e^*,0\right)+D_e^*\\
&A_W=\max\left(F_w^*,0\right)+D_w^*\\
&A_N=\max\left(-F_n^*,0\right)+D_n^*\\
&A_S=\max\left(F_s^*,0\right)+D_s^*\\
&A_p=A_E+A_W+A_N+A_S+\frac{\Omega\left(\frac{\rho_P^*}{J_P^*}\right)^{\tau^*}\Delta V^*}{\Delta\tau^*}\\
&F_e^*=\left(\rho^*G_1{}^*\Delta\eta^{**}\right)_e,F_w^*=\left(\rho^*G_1{}^*\Delta\eta^*\right)_w\\
&F_n^*=\left(\rho^*G_2{}^*\Delta\varsigma^*\right)_n,F_s^*=\left(\rho^*G_2{}^*\Delta\varsigma^*\right)_s\\
&D_e^*=\left(\frac{\Gamma^{\phi^*}J^*\alpha^*\Delta\eta^*}{\Delta\varsigma^*}\right)_e,D_w^*=\left(\frac{\Gamma^{\phi^*}J^*\alpha^*\Delta\eta^*}{\Delta\varsigma^*}\right)_w\\
&D_n^*=\left(\frac{\Gamma^{\phi^*}J^*\gamma^*\Delta\varsigma^*}{\Delta\eta^*}\right)_n,D_s^*=\left(\frac{\Gamma^{\phi^*}J^*\gamma^*\Delta\varsigma^*}{\Delta\eta^*}\right)_s
\end{aligned}\right\} \qquad (21)$$

PRESSURE CORRECTION EQUATION

When solving the momentum equations, the pressure field and density are unknown; therefore the velocity fields obtained after solving the momentum equations generally dose not guarantee the conservation of mass unless the pressure field is

correct. This means that the velocity components such as ($u^*, v^*, w^*, G_1^*, G_2^*$), pressure p* and density ρ* have to correct according to the continuity equation. The velocity components, pressure, and density can be corrected as: -

$$\left.\begin{aligned} u^* &= u^{**} + u'' \\ v^* &= u^{**} + u'' \\ G_1^* &= G_1^{**} + G_1'' \\ G_2^* &= G_2^{**} + G_2'' \\ p^* &= p^{**} + p'' \\ \rho^* &= \rho^{**} + \rho'' \end{aligned}\right\} \quad (22)$$

The details of the pressure correction equation are not mentioned here, and can be found in (**Ahmed, 2005)**, the final form of the pressure correction equation can be written as:-

$$A_P^p p_P'' = A_E^p p_E'' + A_W^p p_W'' + A_N^p p_N'' + A_S^p p_S'' + S_m \quad (23)$$

Where coefficients A involve (α,β,γ, density, etc.) and given in **(Ahmed, 2005),** S_m represents the local imbalance of mass.

SOLUTION PROCEDURE

The description of the entire solution procedure given in this section applies firstly to the steady-state solution. For an unsteady flow this description refers to one time step of the calculations. The steady state solution is started with arbitrary initial guesses for the (ϕ^*) values while the unsteady solution begins with the converged steady values of (ϕ^*) and the advancing to the next time step.

The overall SIMPLE solution procedure takes the following steps: -

- An intermediate velocity field is obtained by solving the momentum equations for u and v. the pressure field obtained from the initial guess.
- The local continuity constraint is enforced by solving equation (23).
- Correct velocities and mass flow rates from equations (22).
- For compressible flow, a constant stagnation enthalpy condition is employed with perfect gas relation to give density.
- Equation (20) is solved for remaining scalar variables, k and ε.
- Iteration from steps 1-5 are repeated until satisfactory convergence is obtained.
- For unsteady flow, steps 1-6 are repeated for the next time step.

RESULTS AND DISCUSSION

The unsteady velocity vector for (Re = $10^5, \Omega = 1$) and for five instants of wake passing ($\tau^* = 0.1, 0.25, 0.5, 0.75$) are shown in **Figs. (4), (5), (6), and (7)** respectively. These figures reveal the development of the stator unsteady field caused by the rotor wake interaction, by referring to these figures and to **Fig.(8)** the incoming wakes create a slip velocity (V_{slip}) directed against downstream blade suction side,

this causes a temporary transport of wake fluid towards the latter. The wake defect is initially uniform **Fig.(4)**, because of the uniform pressure near the pressure side, as the wake moves further in the traverse direction at the passage inlet the wake defect distorted as it approaches to the suction side (this distortion is clearly due to the pressure variations between the two sides) as shown in **Fig(5)** and **Fig(6).** then the wake impinges the suction side blade, further downstream the wake defect after impinging the wake is chopped and transported downstream due to the large convection velocity near the suction side as shown in **Fig.(6)** and **Fig.(7)**.

The unsteady pressure fields ($\Delta p^* = p^* - p^*_{steady}$),(Re = $10^5, \Omega = 1$) for five instants of wake passing ($\tau^* = 0.1, 0.25, 0.5, 0.75$) are shown in **Fig (9), (10), (11),and (12)**. respectively. From these figure it can be noted that the main source of the unsteady pressure is the rotor wake, the wake generates a pressure oscillations on both the pressure and the suction surface. Although that the unsteady pressure magnitude (amplitude) on the pressure side is larger than on the suction side, the fluctuations on the suction side is stronger than the suction side, this can explained by the shorter interaction time on the pressure side. As the wake decay moves toward the suction side and impinges this side at nearly mid axial chord, this impinging generates a zone of high pressure as shown in **Fig.(11)** and **Fig.(12)**.

Fig.(13), and **Fig.(14)** show the comparison of the numerical results with the experimental data at mid-span for steady inflow condition (Ω = 0) and for the time of the wake passing ($\tau^* = 0.75$) respectively. In all the two cases the maximum relative deviation between the numerical results and experimental data is about (25%), the comparison for this complex flow for steady and unsteady is acceptable, in this comparison there is a similar trend between the numerical results and the experimental data, this trend is that in both the numerical results and the experimental data the static pressure on the suction surface decreases and reaches to a minimum value, passing through the minimum pressure and as the fluid particles begin to descend on the rear part of the suction surface, these particle within the boundary layer encounter a positive pressure gradient that causes a separation in that part. Although that there is similar trend between the numerical results and the experimental data, but the behavior of the numerical curve **Fig.(13)** dose not contain a constant pressure region as that shown in the experimental data, the separation zone in the experimental data is characterized by the presence of flat zone in the suction pressure distribution as shown in **Fig.(13)**,(SS $\cong$ 0.62 to SE $\cong$ 0.81) , the reason of this discrepancy is attributed to the deficiency of the standard (k - ε) turbulence model in accurately predicting the flow separation that occurs due to the adverse pressure gradient. Beyond the location ($x^* \cong 0.81$) the fluid reattached and the numerical results with the experimental data are approached.

CONCLUSIONS

Wake passing produces unsteady pressure field in the direction of the rotor traverse. For two-dimensional flow the comparison of the numerical results at mid-span with the experimental data is acceptable and there is similar trend between the prediction and experimental data, except at the separation flow region due to the limitation of the turbulence model.

REFERNCES

- Ahmed, W. M., 2005, "Investigation of the Effect of the Wake Generated by Rotor Blades on the Flow in Stator Passage for Low Pressure Turbine", Ph.D. Thesis, University of Baghdad , Mechanical Engineering Department.

- Denton, D. J., 1983, "An Improved Time-Marching Method for Turbomachinery Flow Calculation", ASME Journal of Engineering for Power, Vol.105, PP 514-520.

- Giles, M. B., 1987, "Calculation of Unsteady Wake/Rotor Interactions", AIAA Paper No. 87-0006.

- Hodson, H. P., 1985, "An Inviscid Blade-to-Blade Prediction of A Wake Generated Unsteady Flow", ASME Journal for Gas Turbines and Power, Vol.107, PP 337-344.

- Hodson, H. P., and Dawes, W. N., 1998, "On the Interpretation of Measured Profile Losses in Unsteady Wake-Turbine Blade Interaction Studies", ASME Journal of Turbomachinery, Vol.120, April, 276-284.

- Launder, B. E., and Spalding, D.B., 1974," The Numerical Computational of Turbulent Flow", Computer Methods in Applied Mechanics and Engineering, Vol.3, PP 269-289.

- Meyer, R. X., 1958, "The Effects of Wakes on the Transient Pressure and Velocity Distributions in Turbomachines", ASME Journal of Basic Engineering, October, PP 1544-1552.

- Parker, R., and Watson, J. F., 1972, "Interaction Effects Between Blade Rows in Turbomachines", Proc. of I. Mech. E., 168, No.21.

- Reda R. M., 1989, "A Study of Unsteady Rotor-Stator Interactions" ASME Journal of Turbomachinery, Vol.111, October, PP 394-400.

- Stieger, R. D., 2002,"The Effects of Wakes on Separating Boundary Layers in Low Pressure Turbine", Ph.D. Thesis, Cambridge University Engineering Department.

NOMENCLATURE
LATIN SYMBOLS

A	Coefficient of the discretized equations
b	Wake width
C_μ	Constant in turbulence model
$C_{\varepsilon 1}$	Constant in turbulence model
$C_{\varepsilon 2}$	Constant in turbulence model
C_d	Drag coefficient of the bars
C_{Ptot}	Total pressure coefficient
C_x	Axial chord of the blade
d	Bar diameter
D	Diffusion at the control volume faces
F	Mass flux at the control volume faces
G_1	Contravariant velocity in ζ direction
G_2	Contravariant velocity in η direction
J	Jacobian transformation
k	Kinetic energy of turbulence
p	Pressure
P_ε	Production of dissipation of K.E. turbulence
P_k	Production of K.E. turbulence
S_ϕ	Source term of ϕ
$S_{\zeta,\eta}$	Source term due to nonorthogonality
S_{total}	Total source terms
t	Time
t_w	Wake passing time
u	Velocity component in x direction
U_{bar}	Velocity of bar
v	Velocity component in y direction
x	Axial coordinate in the physical domain
y	Pitchwise coordinate in the physical domain

GREEK SYMBOLS

α,β,γ	Coordinate transformation parameters
δ_{ij}	Kronecker delta
Δ	Grid spacing
Γ	Diffusion coefficient
ε	Turbulence energy dissipation
μ	Laminar viscosity
μ_t	Turbulent viscosity
ζ,η	Curvilinear coordinates
ρ	Density
$\sigma_{k,}\ \sigma_{\varepsilon}$	Effective Prandtl numbers
τ	Time
τ_{ij}	Reynolds stress tensor
ϕ	Dependent variable
Ω	Reduced frequency

SUBSCRIPTS

e, w, n, s	Values associated with control volume faces
E, W, N, S	Values at neighbor nodes of point p
P	Values at center of the control volume
∞	Value at freestream
i, j	Index Notations or coordinate direction identifiers
oin	Total pressure at inlet
r	Relative frame of reference
slip	Slip velocity
steady	Steady values

SUPERSCRIPTS

'	Fluctuating quantity
*	Dimensionless quantity
''	Corrected values
—	Time-averaged or linear interpolation values

Table(1) Parameters in the General Transport Equation.

Equation	ϕ^*	Γ^*	S_{total}
Continuity	1	0	0
x*-Momentum	$\frac{u}{U_\infty}$	$\frac{1}{\mathrm{Re}}+\mu_t^*$	$-\frac{1}{J^*}\left(\frac{\partial p^*}{\partial x^*}\right)+\frac{1}{J^*}\left[\frac{1}{3}\frac{\partial}{\partial x^*}\left(\Gamma^*\frac{\partial u^*}{\partial x^*}\right)+\frac{\partial}{\partial y^*}\left(\Gamma^*\frac{\partial v^*}{\partial x^*}\right)\right]$ $-\frac{2}{3}\frac{1}{J^*}\left[\frac{\partial}{\partial x^*}\left(\Gamma^*\frac{\partial v^*}{\partial y^*}\right)\right]-\frac{2}{3}\frac{1}{J^*}\frac{\partial}{\partial x^*}\left(\rho^* k^*\right)+S^*_{\varsigma,\eta,u}$
y*-Momentum	$\frac{v}{U_\infty}$	$\frac{1}{\mathrm{Re}}+\mu_t^*$	$-\frac{1}{J^*}\left(\frac{\partial p^*}{\partial y^*}\right)+\frac{1}{J^*}\left[\frac{\partial}{\partial x^*}\left(\Gamma^*\frac{\partial u^*}{\partial y^*}\right)+\frac{1}{3}\frac{\partial}{\partial y^*}\left(\Gamma^*\frac{\partial v^*}{\partial y^*}\right)\right]$ $-\frac{2}{3}\frac{1}{J^*}\left[\frac{\partial}{\partial y^*}\left(\Gamma^*\frac{\partial u^*}{\partial x^*}\right)\right]-\frac{2}{3}\frac{1}{J^*}\frac{\partial}{\partial y^*}\left(\rho^* k^*\right)+S^*_{\varsigma,\eta,v}$
k*	$\frac{k}{U_\infty^2}$	$\frac{1}{\mathrm{Re}}+\frac{\mu_t^*}{\sigma_k}$	$\frac{1}{J^*}\left(P_k^*-\rho^* k^*\right)+S^*_{\varsigma,\eta,k}$
ε*	$\frac{\varepsilon}{U_\infty^3/C_x}$	$\frac{1}{\mathrm{Re}}+\frac{\mu_t^*}{\sigma_\varepsilon}$	$\frac{1}{J^*}\left(C_{\varepsilon 1}\frac{\varepsilon^*}{k^*}P_k^*-\rho^* C_{\varepsilon 1}\frac{\varepsilon^{*2}}{k^*}\right)+S^*_{\varsigma,\eta,\varepsilon}$

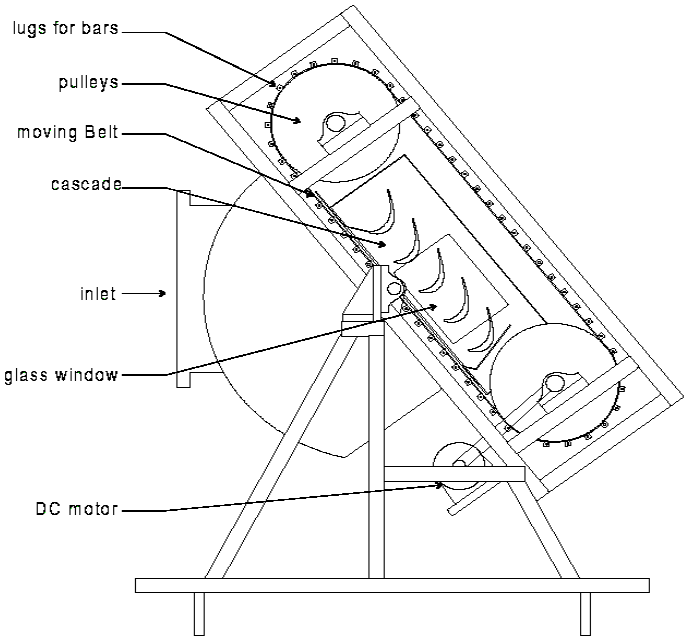

Fig. (1) Bar Passing Cascade Facility Consisting of Wake Generator and Cascade, Stieger (2002).

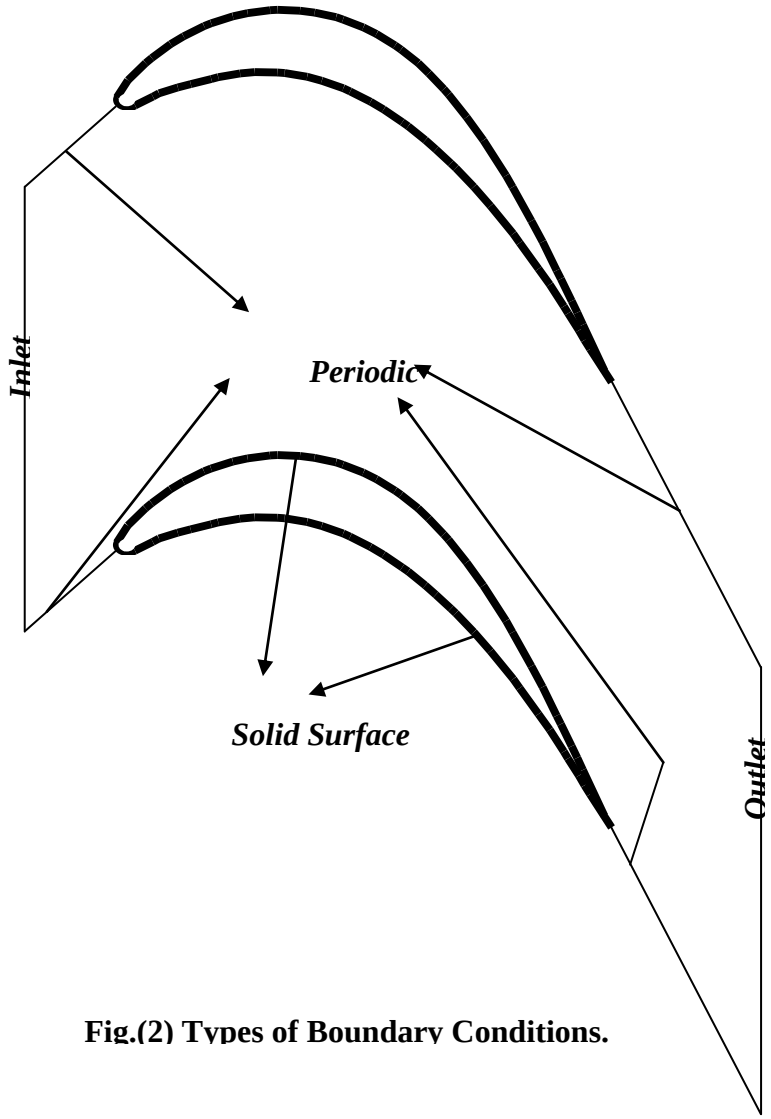

Fig.(2) Types of Boundary Conditions.

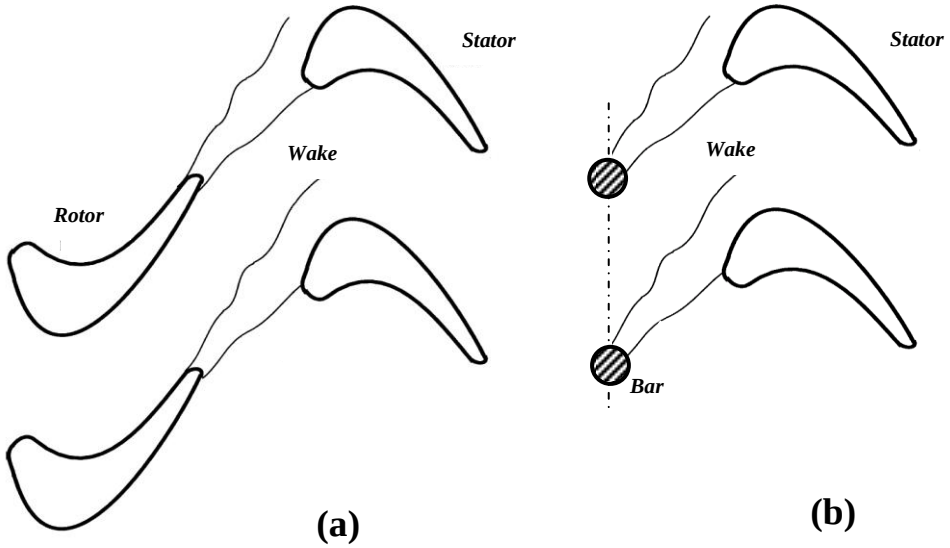

Fig. (3) (a) Schematic or Rotor-Stator wakes Interaction**.**
(b) Simulation of Rotor in **Stieger, 2002,** Experiment**.**

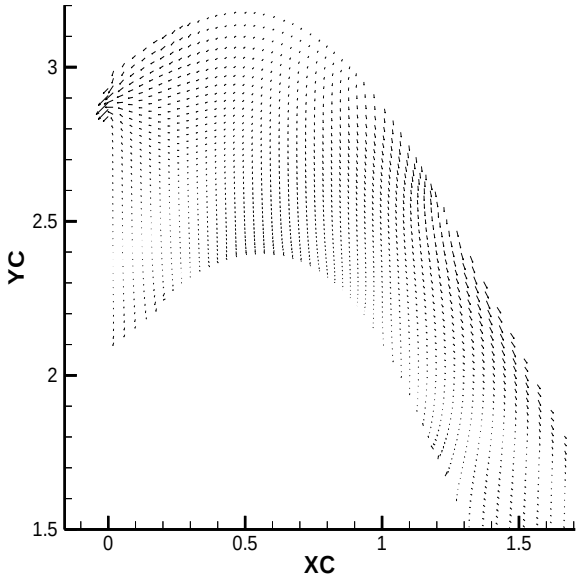

Fig.(4) Unsteady Velocity Vector at Mid-Span at ($\tau^* = 0.1$) for Re = 10^5 ($\Omega = 1$)

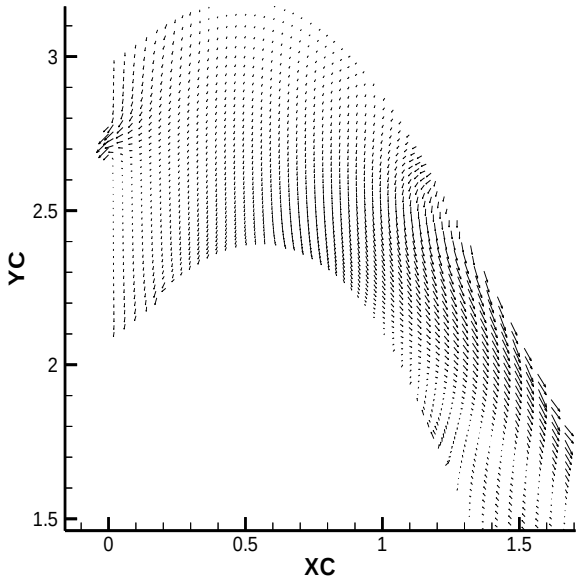

Fig.(5) Unsteady Velocity Vector at Mid-Span at ($\tau^* = 0.25$) for Re = 10^5 ($\Omega = 1$)

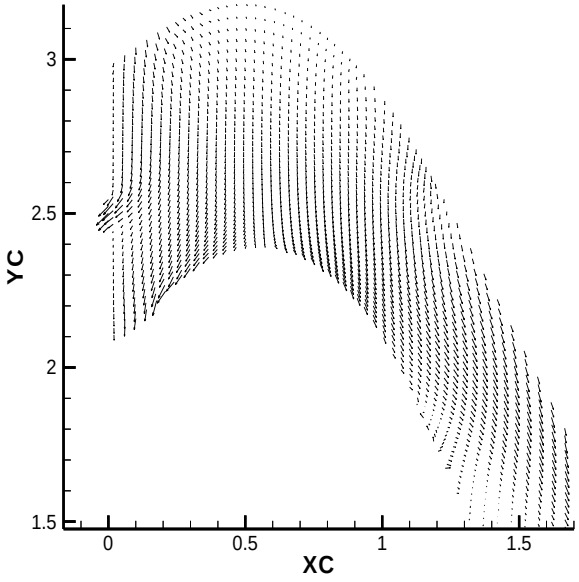

Fig.(6) Unsteady Velocity Vector at Mid-Span at ($\tau^* = 0.5$) for Re = 10^5 ($\Omega = 1$)

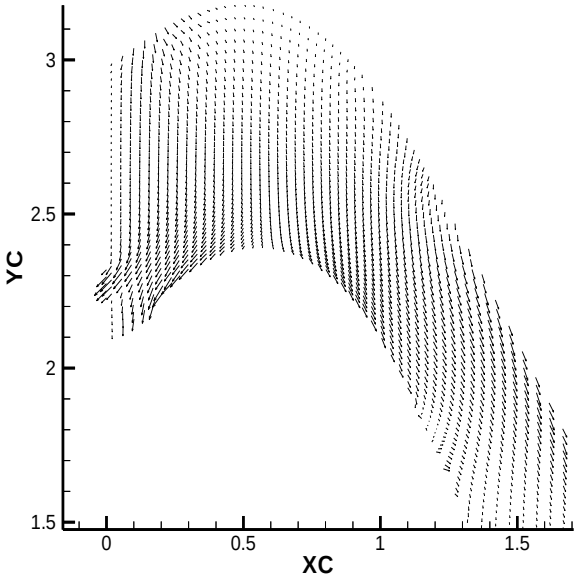

Fig.(7) Unsteady Velocity Vector at Mid-Span at ($\tau^* = 0.75$) for Re = 10^5 ($\Omega = 1$)

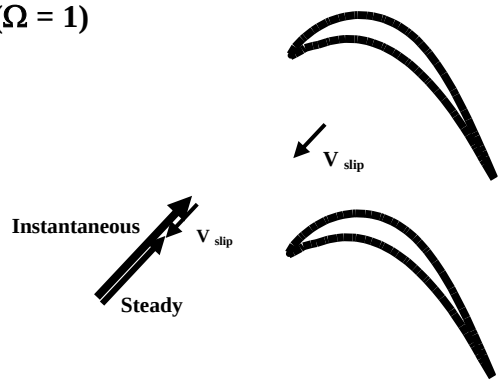

Fig. (8) Instantaneous and Steady Velocities Resulting a Slip Velocity

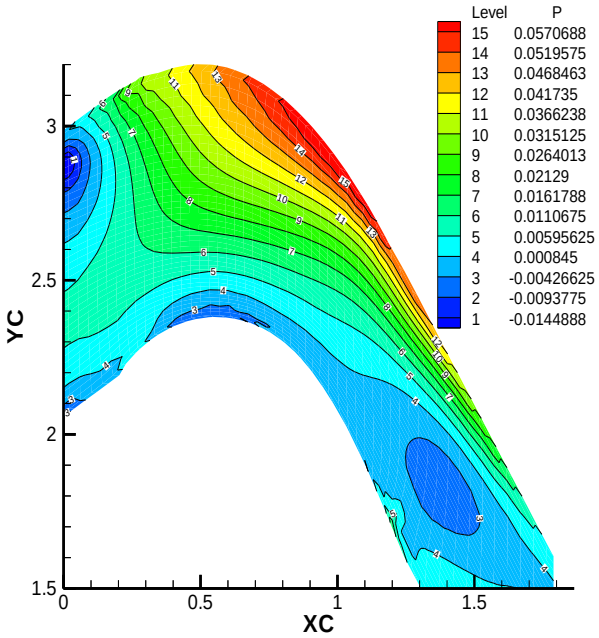

Fig.(9) Unsteady Pressure at Mid-Span at ($\tau^* = 0.1$) for Re = 10^5 ($\Omega = 1$)

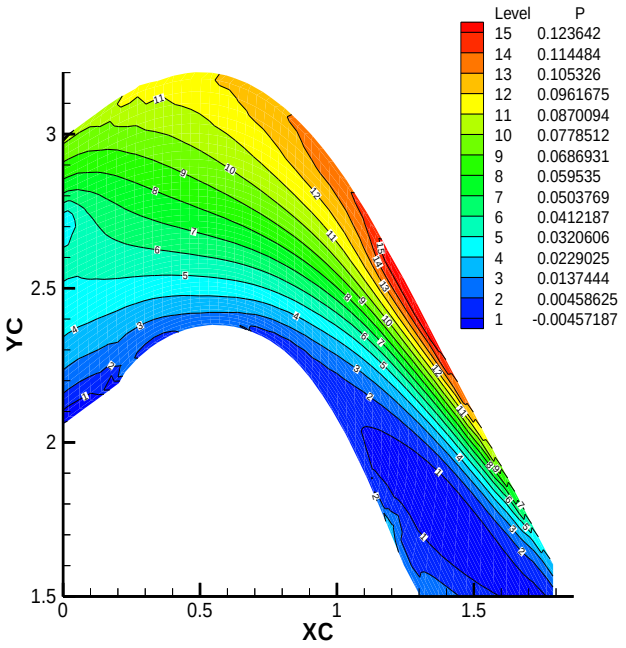

Fig.(10) Unsteady Pressure at Mid-Span at ($\tau^* = 0.25$) for Re = 10^5 ($\Omega = 1$)

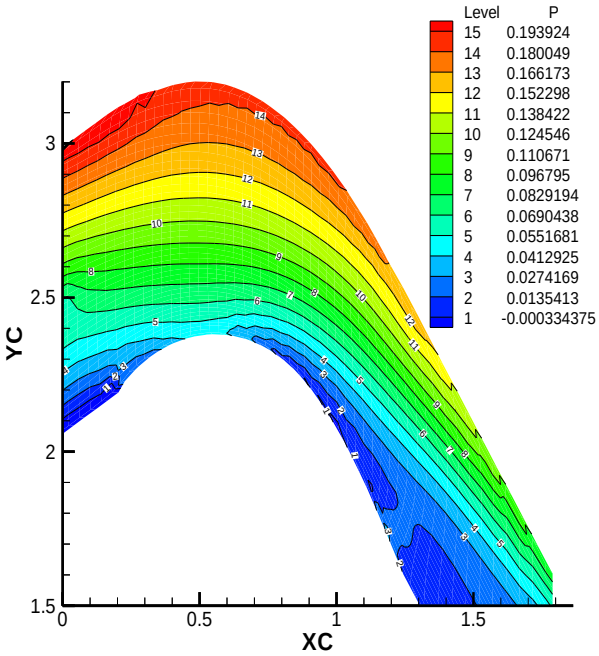

Fig.(11) Unsteady Pressure at Mid-Span at ($\tau^* = 0.5$) for Re = 10^5 ($\Omega = 1$)

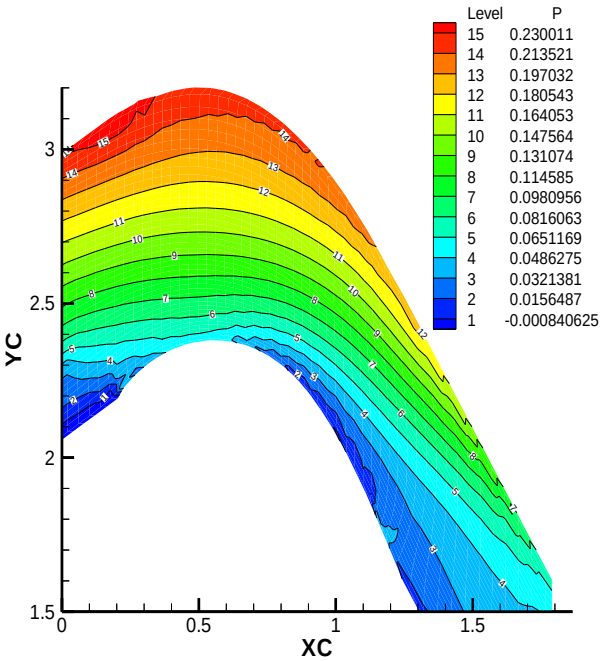

Fig.(12) Unsteady Pressure at Mid-Span at ($\tau^* = 0.75$) for Re = 10^5 ($\Omega = 1$)

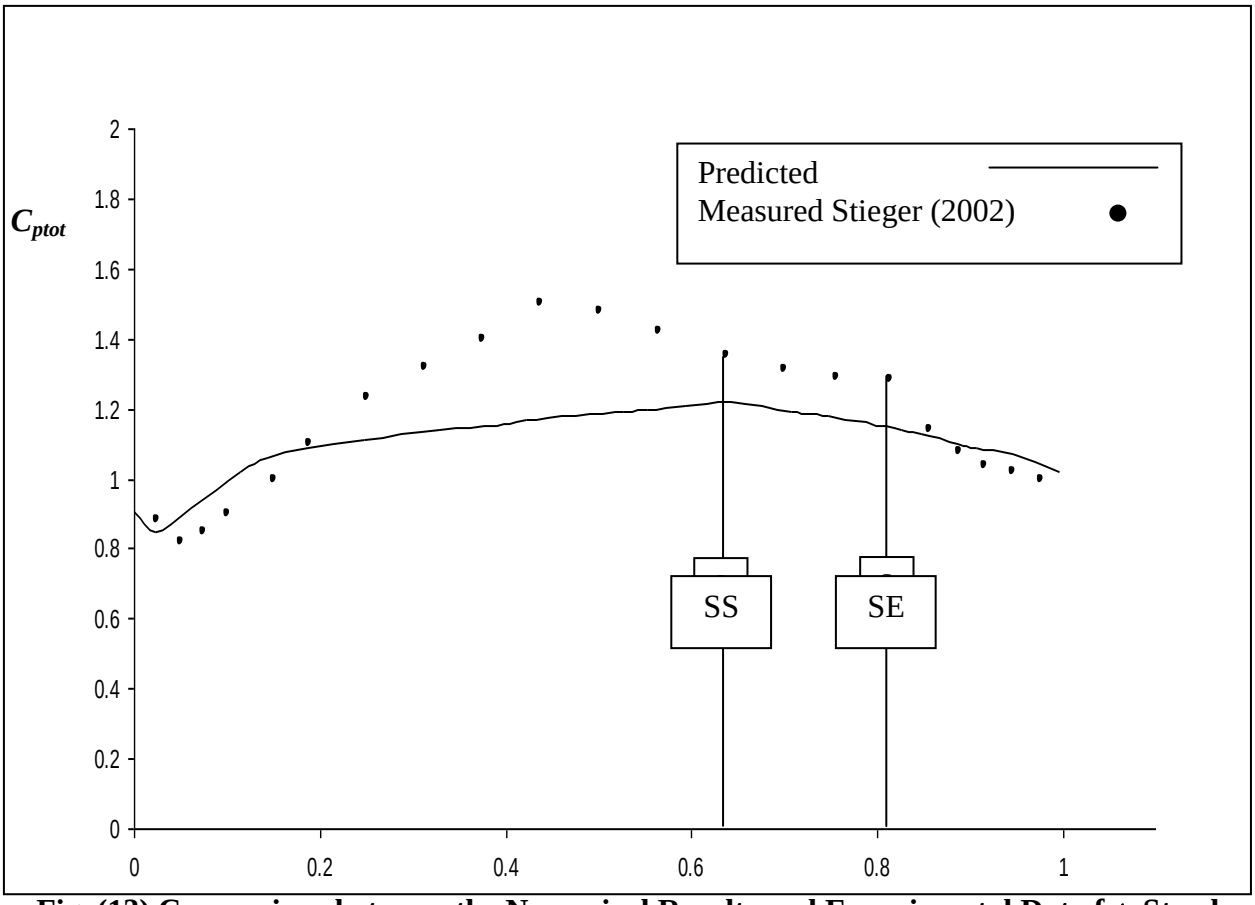

Fig. (13) Comparison between the Numerical Results and Experimental Data for Steady Pressure Coefficient (Re_{2C} = 1.6 x 10^5, Ω = 0) (SS: Separation Start SE: Separation End)

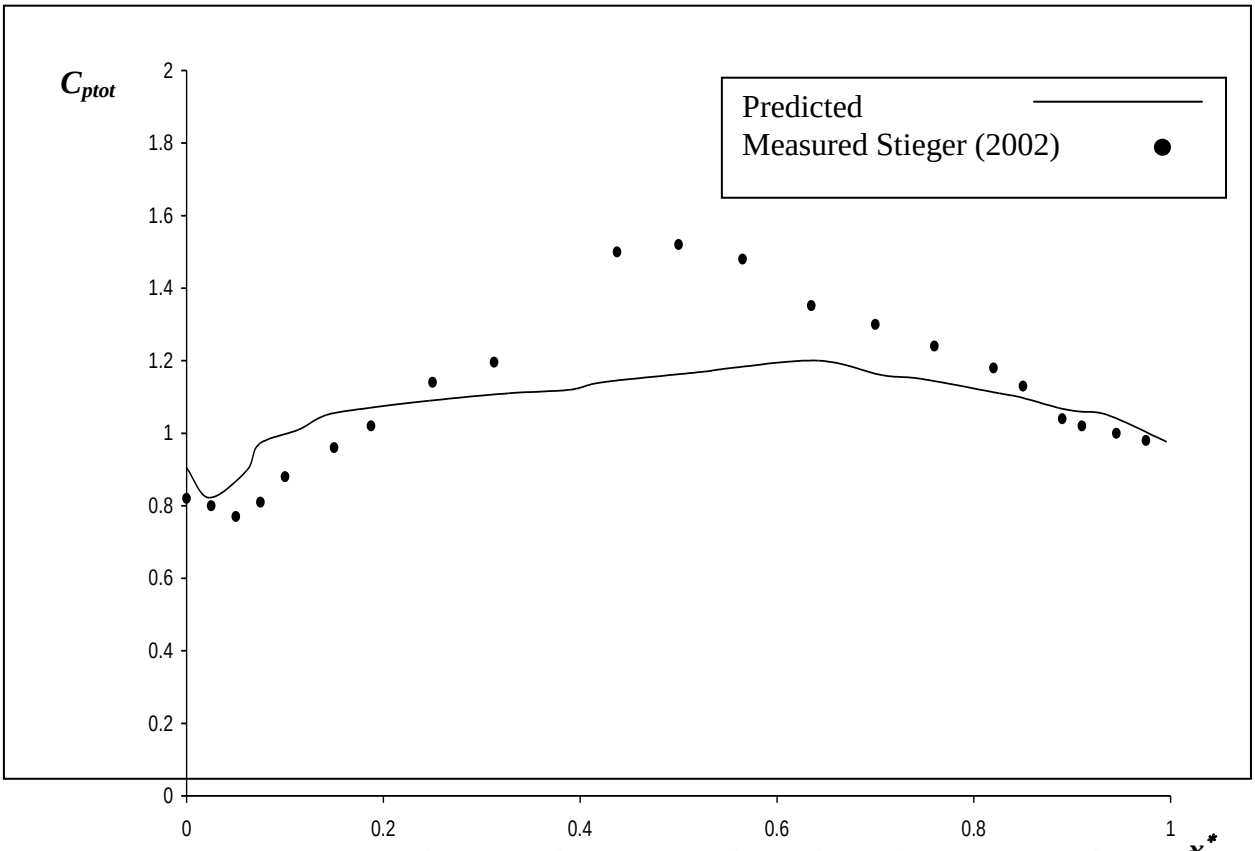

Fig. (14) Comparison between the Numerical Results and Experimental Data for Ensemble Pressure Coefficient at time τ^* = 0.75 (Re_{2C} = 1.6 x 10^5, Ω = 0.68)